Chapter 6

A mathematical model of a two-layered flow in a balloon dilation catheterized oesophageal tube under the influence of peristaltic waves of dilating amplitude: Application to achalasia type swallowing disorder

6.1 Introduction

According to Kahrilas et al. (1995), the oesophageal phase of swallowing is dependent on the contraction and relaxation (called peristalsis) of the oesophageal sphincters as well as the coordinated action of the striated and smooth muscles viz. the longitudinal and circular muscles of the oesophagus. Primary oesophageal peristalsis happens during normal swallowing, while secondary peristalsis refers to introducing a stimulus directly into the oesophagus and eliciting the same kind of motor activity as seen with a full swallow.

Achalasia, which translates to "failure to relax" in Greek, is a rare condition of unclear etiology that is characterized by a failure of the lower esophageal sphincter (LES) to relax and a loss of oesophageal peristalsis (Feldman et al. (2015)). Achalasia affects men and women equally, with a yearly incidence of 1 in 100,000 people and a prevalence of 10 in 100,000 people (Francis and Katzka (2010)). Intermittent dysphagia, with or without weight loss, is a symptom of achalasia.

According to Johnston (2017), oesophageal dysphagia can affect any part of the oesophagus and be classified as structural, propulsive, or mixed-in type. Reflux, food impaction, and chest pain are among its symptoms, which are restricted to the neck or chest. However, it is noteworthy that localization in dysphagia is frequently mixed and nonspecific (Roeder et al. (2004), Johnston (2017)).

Understanding the swallowing mechanism and making an accurate diagnosis is crucial because the management of dysphagia frequently depends on its origin. Treviso-Jones and Skidmore (2015) list endoscopic pneumatic balloon dilatation as one of the treatment possibilities, along with surgical treatments such as Heller's cardiomyotomy, pharmaceutical therapy (nitrates, calcium channel blockers), and, more recently, Peroral Endoscopic Myotomy (POEM). Regarding success rate, procedural simplicity, and complication rates, each of these methods has pros and cons of its own. Pneumatic balloon dilatation is one of the most effective methods. Compared to an oesophagram or modified barium swallow study (MBSS), it offers superior visualization of mucosal lesions and masses and enables direct mucosal biopsies (Levine and Nielsen (1992)).

In order to improve quality of life, achalasia can also be surgically controlled or treated with endoscopic dilatation as a palliative strategy (McCarty and Chao (2021)). When managing strictures or other structural dysphagia of the oesophagus, bougie or balloon dilator endoscopic dilatation is frequently successful; a myotomy is an additional option if the condition is severe (Johnston (2017)).

According to Bhattacharyya (2014) and Wilkins et al. (2007), balloon dilation may be more effective and less likely to cause harm to a patient's oesophagus wall. Nonetheless, it is crucial for patients who have their first endoscopy to validate their diagnosis and rule out the possibility of cancer.

One common method for treating achalasia-related lower oesophageal sphincter issues is Videofluoroscopy-Guided Balloon Dilatation (VGBD) (Pohl et al. (2007)). Additionally, oesophageal and other forms of gastrointestinal strictures are now commonly treated using VGBD. Achalasia and esophageal tumors have been successfully treated by balloon catheter dilatation (Choi et al. (2005), Tatum et al. (2007), Kim et al. (2008)). There is little to no information available about the use of balloon catheter dilatation with catheter insertion into the pharynx or the oesophageal inlet as a recommended, first-line therapy approach for pharyngeal dysphagia (Solt et al. (2001)). Examining the efficacy of upper and lower oesophageal balloon catheter dilatation as a treatment for severe dysphagia is one of the goals of this research.

Many researchers in the area of peristaltically-driven flow have developed mathematical models based on catheterization into arteries (Kanai et al. (1970), Roos and Lykoudis (1971), Wilson et al. (1988), Back et al. (1992), Back (1994), Back et al. (1996), El Misiery et al. (2002b), Hayat et al. (2006), Srivastava (2007), Hayat et al. (2006), Mekheimer et al. (2008), Srivastava and Rastogi (2010), Ledesma et al. (2013)). They all concluded with similar observations regarding pressure distribution inside the considered tube. Consideration of two-layered flow with Newtonian fluid and the conclusion of their studies have been thoroughly discussed in Pandey and Pandey (2024d), where they have put forward a mathematical approach to the pre-diagnosis of swallowing disorders by performing a procedure of catheterization into the oesophagus. In their study, they discussed the pressure distribution along the oesophageal length, the effect of the broadening of a catheter, and the increase in the dilating amplitude parameter on pressure, etc. Further, they have suggested feeding a patient through the mouth who undergoes catheterization via the nose and also feeding may become complicated due to the stimuli of secondary peristalsis into the oesophagus.

Pandey and Pandey (2024b) studied the sliding hiatus hernia and developed a mathematical model of catheterization into the lumen of the oesophagus affected by such a kind of swallowing disorder. The presence of a sliding hiatus hernia in the oesophagus makes its shape bulge. This is one of the reasons for considering the oesophagus as an exponentially diverging tube. They investigated the pressure distribution inside the oesophagus with the catheter. They concluded that less

pressure is required at the lower cardiac sphincter to get the bolus fully inside the stomach.

Now, in this study, we develop a mathematical model of a balloon catheter inserted into the lumen of an oesophagus. For this, we consider a two-layered flow of Newtonian fluids in the core as well as in the periphery region. The flow is driven peristaltically by means of dilating wave amplitude. We require to get answers to the following queries:

(i) What will be the pressure distribution along the oesophageal length?

(ii) Will the pressure distribution pattern be the same throughout the oesophageal length due to the presence of stricture?

(iii) Does the broadening of a catheter still increase the pressure inside the lumen of the oesophagus?

(iv) Does the inflation of the balloon increase the pressure up to its guided length?

(v) At what stages, i.e., insertion, inflation, deflation, or withdrawal, will the pressure get maximum or either be minimum?

And, of course, some more related information will be investigated.

6.2 Mathematical formulation of the problem

We consider the oesophagus with a balloon catheter inserted into it. The oesophagus is assumed to be a cylindrical tube with a two-layered model, i.e., one is the core, and the other is the peripheral. These two layers are carried out by Newtonian fluids with different viscosities, i.e., μ_c for the core and μ_p for the peripheral one. The schematic diagram is shown in Figure 1. In the figure, it has been shown that the balloon inflation is up to length l_1, and the rest part of it is in the deflated condition, i.e., l and $L-(l+l_1)$. The peristaltic sinusoidal wave propagates through the inner and outer walls of the oesophagus, and the dilating wave amplitude is mentioned in the figure (see the dotted lines). To create higher pressure at the distal end of the oesophagus we consider the experimentally verified fact from Kahrilas et al. (1995).

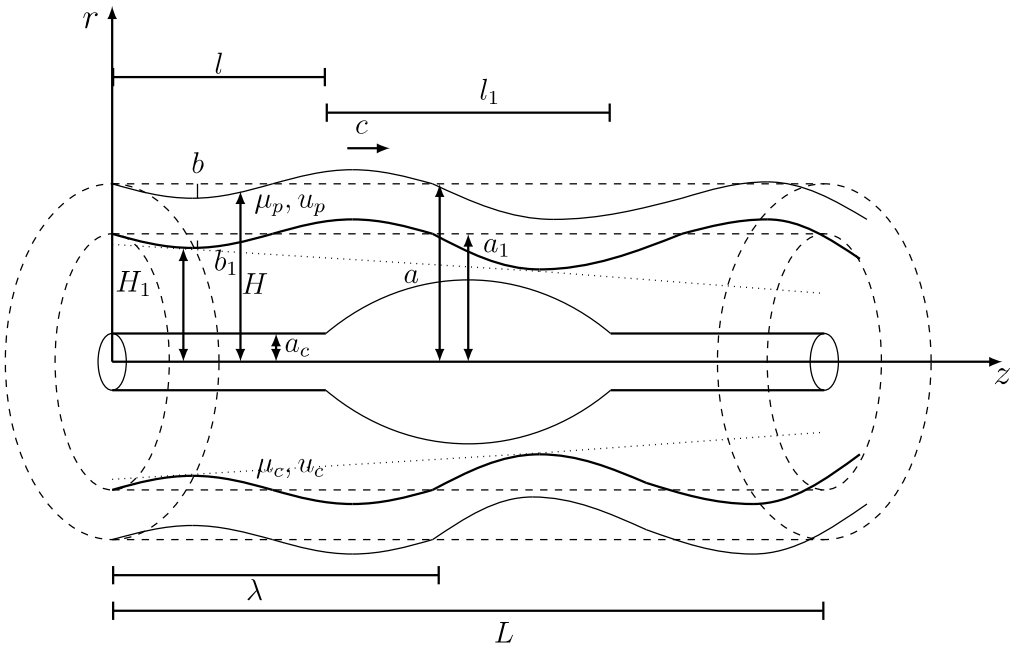

Figure 6.1: The diagram displays the flow of a Newtonian fluid in the two-layer, i.e., the peripheral and the core where a balloon catheter is placed for the dilatation process, and the core layer is surrounded by periphery Newtonian fluid. The light dotted line shows the wave dilation amplitude. The small cylindrical shape is the inflated novel balloon catheter at the distal end of the oesophagus.

It ensures the complete propulsion of the bolus into the stomach, which happens in a normal oesophagus.

The concept of the peristaltic wave with dilating wave amplitude has been experimentally shown in the study of Xia et al. (2009). Pandey et al. (2017) put it in the mathematical formulation and validated it with the experimental results of Xia et al. (2009). Since then, it has been used in many research articles due to its application in oesophagus. Recently, articles related to swallowing disorders and their pre-diagnosis through catheters have been discussed in (Pandey and Pandey (2024d), Pandey and Pandey (2024b)), where this concept of dilating wave amplitude is used. The mathematical formulation of the dilating wave amplitude for the higher pressure at the lower oesophageal sphincter is given by Pandey et al. (2017) as

$$H(Z,t) = a - be^{kZ}\cos^2\frac{\pi}{\lambda}(Z - ct), \tag{6.1}$$

where H, Z, t, a, b, k, λ and c represent respectively the wall displacement, the axial coordinate, time, the tube-radius, the amplitude of the wave, the amplitude dilation parameter, the wavelength, and the wave velocity.

The governing equations are reduced to steady flow when we derive solutions not only in the dimensionless form but also in the wave frame of reference. The transformations, in which the wave frame parameters are on the right side while the laboratory frame parameters are on the left side of the equality signs, are as follows: $Z = z + t$, $R = r$, $U = u + 1$, $V = v$, $p = p$, $\Psi = \psi + r$, $Q = q + 1 = q_c + q_p + 1$, where Ψ, ψ are stream functions, and Q, q are instantaneous volume flow rates, respectively, in the laboratory and the wave frames, with q_c, q_p being the instantaneous flow rates in the core and the peripheral layers respectively.

When we consider axisymmetric flows, the governing equations are free from θ terms. Therefore, Navier Stokes equations, together with the continuity equation for axisymmetric flow through the above-considered geometry where the core layer interacts with the peripheral layer are given by, in cylindrical polar coordinates, as follows:

$$\rho_p\Big(\frac{\partial u_p}{\partial t} + u_p\frac{\partial u_p}{\partial z} + v_p\frac{\partial u_p}{\partial r}\Big) = -\frac{\partial p}{\partial z} + \mu_p\nabla^2 u_p, \quad H_1 \le r \le H, \tag{6.2}$$

$$\rho_p\Big(\frac{\partial v_p}{\partial t} + u_p\frac{\partial v_p}{\partial z} + v_p\frac{\partial v_p}{\partial r}\Big) = -\frac{\partial p}{\partial r} + \mu_p(\nabla^2 - \frac{1}{r^2})v_p, \quad H_1 \le r \le H, \tag{6.3}$$

$$\frac{1}{r}\frac{\partial}{\partial r}(rv_p) + \frac{\partial}{\partial z}(u_p) = 0. \tag{6.4}$$

For the core layer,

$$\rho_c\Big(\frac{\partial u_c}{\partial t} + u_c\frac{\partial u_c}{\partial z} + v_c\frac{\partial u_c}{\partial r}\Big) = -\frac{\partial p}{\partial z} + \mu_c\nabla^2 u_c, \quad a_c \le r \le H_1, \tag{6.5}$$

$$\rho_c\Big(\frac{\partial v_c}{\partial t} + u_c\frac{\partial v_c}{\partial z} + v_c\frac{\partial v_c}{\partial r}\Big) = -\frac{\partial p}{\partial r} + \mu_c(\nabla^2 - \frac{1}{r^2})v_c, \quad a_c \le r \le H_1, \tag{6.6}$$

$$\frac{1}{r}\frac{\partial}{\partial r}(rv_c) + \frac{\partial}{\partial z}(u_c) = 0. \tag{6.7}$$

$\nabla^2 \equiv \frac{\partial^2}{\partial r^2} + \frac{1}{r}\frac{\partial}{\partial r} + \frac{\partial^2}{\partial z^2}$ is the Laplacian operator, r is the radial coordinate and p is the pressure. In the peripheral region u_p, v_p are the components of velocity and ρ_p is

the fluid density, respectively, whereas in the core region u_c, v_c are the components of velocity and ρ_c is the fluid density.

The interface between the core layer and the peripheral layer is given by Brasseur et al. (1987) as $H_1 = a_1 - b_1 e^{kZ} \cos^2 \frac{\pi}{\lambda}(Z - ct)$, where the amplitude for this interface wave is b_1. Non-dimensional variables are as follows
$(u_p', u_c') = \frac{(u_p, u_c)}{c}$, $r' = \frac{r}{a}$, $k' = k\lambda$, $b' = \frac{b}{a}$, $z' = \frac{z}{\lambda}$, $t' = \frac{ct}{\lambda}$, $(v_p', v_c') = \lambda \frac{(u_p, u_c)}{ac}$, $p' = \frac{a^2 p}{\lambda c \mu_c}$, $\mu = \frac{\mu_p}{\mu_c}$, using these variables from equations (6.2) to (6.7), we get
for the peripheral layer $(h_1 \leq r \leq h)$

$$\delta Re\Big(\frac{\partial u_p}{\partial t} + u_p \frac{\partial u_p}{\partial z} + v_p \frac{\partial u_p}{\partial r}\Big) = -\frac{\partial p}{\partial z} + \mu\Big(\frac{1}{r}\frac{\partial}{\partial r}(r\frac{\partial u_p}{\partial r}) + \delta^2 \frac{\partial^2 u_p}{\partial z^2}\Big), \tag{6.8}$$

$$\delta^3 Re\Big(\frac{\partial v_p}{\partial t} + u_p \frac{\partial v_p}{\partial z} + v_p \frac{\partial v_p}{\partial r}\Big) = -\frac{\partial p}{\partial r} + \mu\Big(\delta^2 \frac{1}{r}\frac{\partial}{\partial r}(r\frac{\partial v_p}{\partial r}) + \delta^4 \frac{\partial^2 v_p}{\partial z^2} - \delta^2 \frac{v_p}{r^2}\Big), \tag{6.9}$$

$$\frac{1}{r}\frac{\partial}{\partial r}(r v_p) + \frac{\partial u_p}{\partial z} = 0, \tag{6.10}$$

and for the core layer $(\epsilon \leq r \leq h_1)$

$$\Big(\frac{\rho_c}{\rho_p}\Big) Re\delta\Big(\frac{\partial u_c}{\partial t} + u_c \frac{\partial u_c}{\partial z} + v_c \frac{\partial u_c}{\partial r}\Big) = -\frac{\partial p}{\partial z} + \mu\Big(\frac{1}{r}\frac{\partial}{\partial r}(r\frac{\partial u_c}{\partial r}) + \delta^2 \frac{\partial^2 u_c}{\partial z^2}\Big), \tag{6.11}$$

$$\Big(\frac{\rho_c}{\rho_p}\Big) Re\delta^3\Big(\frac{\partial v_c}{\partial t} + u_c \frac{\partial v_c}{\partial z} + v_c \frac{\partial v_c}{\partial r}\Big) = -\frac{\partial p}{\partial r} + \mu\Big(\delta^2 \frac{1}{r}\frac{\partial}{\partial r}(r\frac{\partial v_c}{\partial r}) + \delta^4 \frac{\partial^2 v_c}{\partial z^2} - \delta^2 \frac{v_c}{r^2}\Big), \tag{6.12}$$

$$\frac{1}{r}\frac{\partial}{\partial r}(r v_c) + \frac{\partial u_c}{\partial z} = 0, \tag{6.13}$$

where
$h = \frac{H}{a} = 1 - \phi e^{k(z+t)} \cos^2(\pi z)$;
$h_1 = \frac{H_1}{a} = \alpha - \phi_1 e^{k(z+t)} \cos^2(\pi z)$; $\epsilon = \frac{a_c}{a}$; $(\alpha, \phi, \phi_1) = (a_1, b, b_1)/a$; $Re = \frac{\rho_p a c}{\mu_c}$; $\delta = \frac{a}{\lambda}$.
Here Re and δ are the Reynolds and the wave number respectively.
Using the assumptions of low Reynolds number and large wavelength approximations and ignoring the terms of inertia, we get equations (6.8)-(6.13) simplified as

$$\frac{\partial p}{\partial z} = \frac{1}{r}\frac{\partial}{\partial r}\Big(r\mu \frac{\partial}{\partial r}\Big) u_p, \quad h_1 \leq r \leq h, \tag{6.14}$$

$$\frac{\partial p}{\partial z} = \frac{1}{r}\frac{\partial}{\partial r}\Big(r \frac{\partial}{\partial r}\Big) u_c, \quad \epsilon \leq r \leq h_1. \tag{6.15}$$

The non-dimensional boundary conditions are described as follows

$$u_p = -1 \quad at \quad r = h, \tag{6.16}$$

$$u_c = -1 \quad at \quad r = j_1 + j\,\mathrm{sech}\left(\frac{(z-\gamma)^2}{\gamma_1}\right) = \epsilon, \tag{6.17}$$

$$u_p = u_c \quad at \quad r = h_1. \tag{6.18}$$

No-slip condition on the tube wall and velocity continuity at the interface are specified in equations (6.16) to (6.18).

6.3 Solutions

The peripheral and the core layers velocities can be obtained by integrating equations (6.14) and (6.15), under the conditions (6.16) to (6.18), as follows

$$u_p = -1 - \frac{1}{4\mu}\frac{dp}{dz}\Big[h^2 - r^2 + M\log\left(\frac{r}{h}\right)\Big], \tag{6.19}$$

$$u_c = -1 - \frac{1}{4}\frac{dp}{dz}\Big[(j_1 + j\,\mathrm{sech}(\frac{(z-\gamma)^2}{\gamma_1}))^2 - r^2 + M\log\left(\frac{r}{j_1 + j\,\mathrm{sech}(\frac{(z-\gamma)^2}{\gamma_1})}\right)\Big], \tag{6.20}$$

with

$$M = \frac{-h^2 + \mu(j_1 + j\,\mathrm{sech}(\frac{(z-\gamma)^2}{\gamma_1}))^2 + (1-\mu)h_1^2}{\log(\frac{h_1}{h}) - \mu\log(\frac{h_1}{j_1 + j\,\mathrm{sech}(\frac{(z-\gamma)^2}{\gamma_1})})}.$$

The criteria can be used to obtain solutions in terms of stream functions as $\psi_c = 0$ at $r = 0$ and $\psi_p = \frac{q}{2}$ at $r = h$ (Rao and Usha (1995), Usha and Ramachandra Rao (1997)) in equations (6.19) and (6.20). Applying the criteria, we get
for $h_1 \le r \le h$,

$$\psi_p = \frac{q + h^2 - r^2}{2} + \frac{1}{4\mu}\frac{dp}{dz}\Big[\Big(\frac{h^4 + r^4}{4}\Big) - \frac{r^2h^2}{2} - M\Big\{\frac{h^2}{4} + \frac{r^2}{2}\Big(\log\left(\frac{r}{h}\right) - \frac{1}{2}\Big)\Big\}\Big], \tag{6.21}$$

and for $j_1 \le r \le h_1$,

$$\psi_c = \frac{r^2}{2}\Big[-1 - \frac{1}{4}\frac{dp}{dz}\Big\{(j_1 + j\,\mathrm{sech}(\frac{(z-\gamma)^2}{\gamma_1}))^2 - \frac{r^2}{2} + M\Big\{\log\left(\frac{r}{j_1 + j\,\mathrm{sech}(\frac{(z-\gamma)^2}{\gamma_1})}\right) - \frac{1}{2}\Big\}\Big\}\Big]. \tag{6.22}$$

Thus, we can see that if $\mu \to 1$ in the absence of catheter equations (6.21) and (6.22) reduce to Newtonian fluid and for a single fluid case obtained by (Rao and Usha (1995), Usha and Ramachandra Rao (1997)) respectively.
Now using the condition $\psi_p = \frac{q_c}{2}$ at $r = h_1$ (Rao and Usha (1995), Usha and Ramachandra Rao (1997)) in equation (6.21), we get

$$\frac{q_c + h_1^2}{2} = \frac{q + h^2}{2} + \frac{1}{4\mu}\frac{dp}{dz}\Big[\Big(\frac{h^4 + h_1^4}{4}\Big) - \frac{h_1^2 h^2}{2} - M\Big\{\frac{h^2}{4} + \frac{h_1^2}{2}\Big(\log\Big(\frac{h_1}{h}\Big) - \frac{1}{2}\Big)\Big\}\Big], \quad (6.23)$$

which is a fourth-degree equation in h_1, a streamline in the flow field.

Also using the condition $\psi_c = \frac{q_c}{2}$ at $r = h_1$ in equation (6.22), we get

$$\begin{aligned}\frac{q_c + h_1^2}{2} = & -\frac{1}{4}\frac{dp}{dz}\Big[\frac{h_1^2(j_1 + j\,\mathrm{sech}(\frac{(z-\gamma)^2}{\gamma_1}))^2}{2} - \frac{h_1^4}{4} \\ & + M\Big\{\frac{h_1^2}{2}\Big(\log\Big(\frac{h_1}{j_1 + j\,\mathrm{sech}(\frac{(z-\gamma)^2}{\gamma_1})}\Big) - \frac{1}{2}\Big)\Big\}\Big].\end{aligned} \quad (6.24)$$

It is to be noted that the right side expressions in (6.23) and (6.24) are equal and will lead to the determination of quantities such as the volume flow rate, etc., in terms of h_1 and q_c.

Instantaneous volume flow rate is thus obtained from (6.23) and (6.24) as

$$\begin{aligned}q = & -h^2 - \frac{1}{8\mu}\frac{dp}{dz}\Big[h^4 + (1-\mu)h_1^4 + 2h_1^2(\mu(j_1 + j\,\mathrm{sech}(\frac{(z-\gamma)^2}{\gamma_1}))^2 - h^2) \\ & + M\Big\{-h^2 + (1-\mu)h_1^2 + 2h_1^2 B\Big\}\Big],\end{aligned} \quad (6.25)$$

where $B = \Big(\mu\log(\frac{h_1}{j_1 + j\,\mathrm{sech}(\frac{(z-\gamma)^2}{\gamma_1})}) - \log(\frac{h_1}{h})\Big)$.
Using equation (6.24) we write

$$\begin{aligned}q_c = & -h_1^2 - \frac{1}{8}\frac{dp}{dz}\Big[-h_1^4 + 2h_1^2(j_1 + j\,\mathrm{sech}(\frac{(z-\gamma)^2}{\gamma_1}))^2 \\ & + 2M\Big\{h_1^2\Big(\log\Big(\frac{h_1}{j_1 + j\,\mathrm{sech}(\frac{(z-\gamma)^2}{\gamma_1})}\Big) - 1\Big)\Big\}\Big].\end{aligned} \quad (6.26)$$

Since the expression for flow rate q has been found in (6.25), we write

$$\frac{dp}{dz} = \frac{-8\mu(h^2+q)}{\eta}, \tag{6.27}$$

where $\eta = h^4 + (1-\mu)h_1^4 + 2h_1^2(\mu(j_1 + j\,\mathrm{sech}(\frac{(z-\gamma)^2}{\gamma_1}))^2 - h^2) + M\Big\{-h^2 + (1-\mu)h_1^2 + 2h_1^2 B\Big\}$

Following Brasseur et al. (1987), by taking $h_1 = \alpha$ and $h = 1$, we rewrite $\tilde{\eta}$ as

$$\tilde{\eta} = [1 + (1-\mu)\alpha^4 + 2\alpha^2(\mu(j_1 + j\,\mathrm{sech}(\frac{(z-\gamma)^2}{\gamma_1}))^2 - 1) + N\{-1 + (1-\mu)\alpha^2 + 2\alpha^2 C\}],$$

where $C = \mu\log(\alpha/(j_1 + j\,\mathrm{sech}(\frac{(z-\gamma)^2}{\gamma_1}))) - \log(\alpha)$ and $N = \frac{-1+\mu(j_1+j\,\mathrm{sech}(\frac{(z-\gamma)^2}{\gamma_1}))^2+(1-\mu)\alpha^2}{\log(\alpha)-\mu\log(\alpha/(j_1+j\,\mathrm{sech}(\frac{(z-\gamma)^2}{\gamma_1})))}$.

The pressure is given by

$$\Delta p = \int_0^z \frac{8\mu(q+h^2)}{\eta}dz.$$

Using the expression for wall surface given in equation (6.1) we find, in view of (6.1),

$$\Delta p = \int_0^z \frac{8\mu}{\eta}(q + 1 - 2\phi e^{k(z+t)}\cos^2(\pi z) + \phi^2 e^{2k(z+t)}\cos^4(\pi z))dz,$$

Symbolising $I_1 = \displaystyle\int_0^z \frac{1}{\eta}dz$, $I_2 = \displaystyle\int_0^z \frac{e^{k(z+t)}\cos^2(\pi z)}{\eta}dz$, and

$I_3 = \displaystyle\int_0^z \frac{e^{2k(z+t)}\cos^4(\pi z)}{\eta}dz$, in view of this, we write the above equation as

$$\Delta p = 8\mu[(q+1)I_1 - 2\phi I_2 + \phi^2 I_3]. \tag{6.28}$$

The time-averaged volume flow rate, $\overline{Q}$, is given by

$$\overline{Q} = (q+1) - 2\phi e^{kz}\Big(\frac{e^k - 1}{k}\Big) + \phi^2 e^{2kz}\Big(\frac{e^{2k}-1}{2k}\Big), \tag{6.29}$$

which, for k, reduces to that for uniform wave amplitude.

Therefore, using equations (6.28) and (6.29), we get

$$\Delta p = 8\mu\Big[\Big(\overline{Q} + 2\phi e^{kz}\Big(\frac{e^k-1}{k}\Big) - \phi^2 e^{2kz}\Big(\frac{e^{2k}-1}{2k}\Big)\Big)I_1 - 2\phi I_2 + \phi^2 I_3\Big]. \tag{6.30}$$

The pressure that must be applied to achieve $\overline{Q} = 0$ is given by

$$\Delta p_0 = 8\mu\Big[\Big(2\phi e^{kz}\Big(\frac{e^k-1}{k}\Big) - \phi^2 e^{2kz}\Big(\frac{e^{2k}-1}{2k}\Big)\Big)I_1 - 2\phi I_2 + \phi^2 I_3\Big], \tag{6.31}$$

which also, for $k = 0$, reduces to that for uniform wave amplitude.

From equation (6.30), we deduce $\overline{Q}$ as

$$\overline{Q} = \frac{\Delta p}{8\mu I_1} + 2\phi\frac{I_2}{I_1} - 2\phi e^{kz}\Big(\frac{e^k-1}{k}\Big) + \phi^2 e^{2kz}\Big(\frac{e^{2k}-1}{2k}\Big) - \phi^2\frac{I_3}{I_1}. \tag{6.32}$$

The time-averaged flow rate at zero pressure is given by

$$\overline{Q}_0 = 2\phi\frac{I_2}{I_1} - \phi^2\frac{I_3}{I_1} - 2\phi e^{kz}\Big(\frac{e^k-1}{k}\Big) + \phi^2 e^{2kz}\Big(\frac{e^{2k}-1}{2k}\Big). \tag{6.33}$$

From equations (6.32) and (6.33), we get

$$\Delta p = (\overline{Q} - \overline{Q}_0)8\mu I_1, \tag{6.34}$$

from equations (6.31) and (6.33)

$$\Delta p_0 = -8\mu\overline{Q}_0 I_1. \tag{6.35}$$

and thus from (6.34) and (6.35)

$$\overline{Q} = \overline{Q}_0\Big(1 - \frac{\Delta p}{\Delta p_0}\Big). \tag{6.36}$$

The friction force $F_a(= f_a/\pi\lambda c\mu_p)$ at the tube wall across the axial length is now obtained as

$$F_a = \int_0^z h^2\Big(-\frac{dp}{dz}\Big)dz. \tag{6.37}$$

Therefore,

$$F_a = 8\mu\Big(A_1 + (\overline{Q}-1)A_2 + 2\phi\Big(\frac{e^k-1}{k}\Big)A_3 - \phi^2\Big(\frac{e^{2k}-1}{2k}\Big)A_4\Big), \tag{6.38}$$

where, $A_1 = \int_0^z \frac{h^4}{\eta} dz$, $A_2 = \int_0^z \frac{h^2}{\eta} dz$, $A_3 = \int_0^z \frac{h^2}{\eta} e^{kz} dz$ and $A_4 = \int_0^z \frac{h^2}{\eta} e^{2kz} dz$.

The friction force $F_c (= f_c/\pi\lambda c\mu_c)$ at the catheter wall across the axial length is now derived as

$$F_c = \int_0^z (j_1 + j\,\mathrm{sech}(\frac{(z-\gamma)^2}{\gamma_1}))^2 \Big(- \frac{dp}{dz}\Big) dz. \tag{6.39}$$

Thus,

$$F_c = 8\mu(j_1 + j\,\mathrm{sech}(\frac{(z-\gamma)^2}{\gamma_1}))^2 \Big[(\overline{Q} - 1)B_1 + \phi\Big(\frac{e^k - 1}{k}\Big)B_2 - \phi^2\Big(\frac{e^{2k} - 1}{2k}\Big)B_3 + B_4 \Big], \tag{6.40}$$

where $B_1 = \int_0^z \frac{1}{\eta} dz$, $B_2 = \int_0^z \frac{e^{kz}}{\eta} dz$, $B_3 = \int_0^z \frac{e^{2kz}}{\eta} dz$ and $B_4 = \int_0^z \frac{h^2}{\eta} dz$.
It should be noted that the results for a single-phase Newtonian viscous fluid are obtained with $\alpha = 1$ and $\mu = 1$. Using $\alpha = 1$, $\mu = 1$, for the no catheter case, the results of Shapiro et al. (1969) are recovered from the current study.

6.4 Results and discussions

In this section, we present and discuss the results of various parameters set up to give way to read achalasia with various fixed parameters. Some of these findings are consistent with the literature, while others have no experimental counterpart for validation. However, they serve the purpose of predictions.

Various flow parameters are considered for the purpose of the study, and the practicality of these parametric values is their foundational aspect. These are all given in non-dimensional form, granting us the flexibility to select values within specific ranges. In determining these parameters, we followed the methodology outlined by Brasseur et al. (1987) in their published work. For instance, the symbol α represents the ratio of peripheral layer thickness to the tube radius. As a result, α falls within the range of 0 to 1, where 0 signifies the absence of a peripheral layer, while 1 indicates the absence of a core layer. The figures illustrate that the practical range for α is typically below 0.4. However, it's important to note that our analysis is primarily qualitative. When examining the influence of viscosity on peripheral layers,

we use a value of 0.4 solely for clarity. In certain instances, we choose 0.2 for the same reason. As for the symbol ϕ, which represents dimensionless wave amplitude, it can take values from 0 to 1. Based on anatomical measurements by Xia et al. (2009), the estimated dimensionless ϕ ranges from 0.47 to 0.8043, corresponding to a value of k equal to 0.134. For clarity, we assume that k is less than 0.1, which is a reasonable approximation. The value ϵ, i.e., the diameter of the balloon catheter, is assigned as 0.1, which is considered ideal (Said et al. (2003)). All detailed calculations are available in the appendix of Pandey et al. (2017) publication.

Achalasia in the oesophagus is modeled under balloon catheter dilatation, which is used for diagnosing achalasia in patients. Endoscopic balloon dilation has been recommended as a first-line treatment in these cases. It has also been proven safe and reliable (Oxford and Ducic (2006)). The research from the biomedical science point of view has given the observed results for the higher pressure at the upper and lower oesophageal sphincters (Hu et al. (2022)), which creates discomfort to the patient. We tried to find a way to overcome the pressure on the sphincters by formulating mathematically. Also, getting maximum and minimum pressures to inflate and deflate the balloon catheter (Solt et al. (2001), Solt et al. (2004), Kim et al. (2008), Blount et al. (2010)) into the oesophagus are thoroughly summarised in this study. To serve the purpose we plot graphs for various purposes, such as to learn the impact of an inserted balloon catheter on pressure distribution throughout the oesophagus, to gain knowledge about the effect of dilating wave amplitude, and to read the peripheral layer velocity profile and the change in pressure difference with the averaged volume flow rate.

We discuss with a proper understanding of how pressure distributes in the essential structures for the biological development of dysphagia. Through this study, it is crucial to identify the key factors that exclude the presence of a possible malignancy and influences already existing high pressure in the oesophagus. This paper's primary objective is to discuss and explore the influence of inflation and deflation with the inserted balloon catheter and also to compare this study on flow dynamics, such as pressure distribution, with the results to that of Pandey et al. (2017), Pandey and Pandey (2024c) without catheter, and (Pandey and Pandey (2024d); Pandey and Pandey (2024b), Pandey and Pandey (2024a)) with the introduced catheter.

The balloon catheter in the core layer of the oesophagus may be placed anywhere from the proximal to the distal end. Initially, we observed that introducing the deflated balloon catheter into the oesophagus to broaden the stricture creates higher pressure. As it progresses towards the stricture site, pressure decreases, and it rises to push the bolus forward. The placement of the deflated balloon catheter just before the site of the present stricture reduces the pressure. However, the pressure increases sharply as the inflation of the balloon starts. This pressure is maximum when the balloon is fully inflated. It is concluded that the pressure is high due to the stuck flow and catheter insertion before the stricture site. However, pressure and flow decreased as the balloon inflated completely at the stricture site. Moreover, it is interesting to note that the broadening of the size of a catheter leads to higher pressure with the same balloon size.

We consider the position of stricture at the distal end of the oesophagus. However, we can also shift as we change the value of j_1, j, γ, and γ_1 to inflate the balloon. In Figures 6.2(a-e), we observed that the pressure spikes as we inflate the balloon into the oesophagus at the affected junction. This is validated with the experimental results given by Kiousis et al. (2009) for arteries, whereas for a diagnosis of the oesophagus in biomedical by Hu et al. (2022), and computationally and numerically, results by Akhtar et al. (2023) during the diagnosis of a patient through a balloon catheter. Initially, due to high pressure at the Upper Oesophageal Sphincter (UES), the valve is closed, and the same is shown at the crest in the graph. As the deflated balloon catheter is inserted, the pressure at the upper sphincter is released, as shown at the graph's trough. This process continues until it reaches the position where the balloon catheter is finally placed. At this junction, we observe a larger growth in the magnitude of pressure, which shows that a higher pressure is required to let the flow pass through it. The results of Akhtar et al. (2023) validate this. The value of ϵ demonstrates that the pressure gets higher as the balloon inflates, and at the same time, it opposes the existing pressure. In comparison to the study of Pandey et al. (2017) without a catheter, and (Pandey and Pandey (2024d); Pandey and Pandey (2024b)) with the catheter, we can see a large impact of the broadening of the catheter on the pressure distribution into the oesophagus in this study. We also observe that using a balloon catheter helps minimize the risk of perforation caused by inappropriate advancement of instruments and misplacement of the balloon during its inflation caused by sliding and gives a real-time stricture dilation

during balloon inflation compared to normal catheterization.

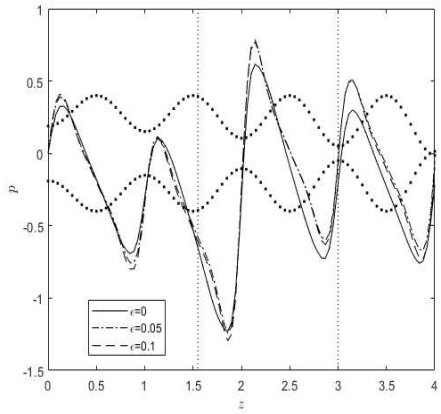

(a)

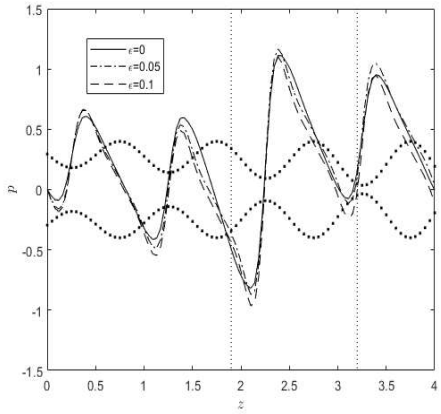

(b)

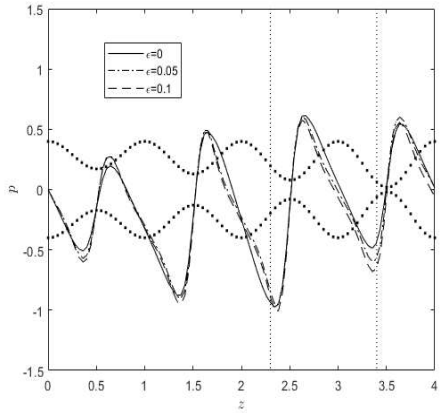

(c)

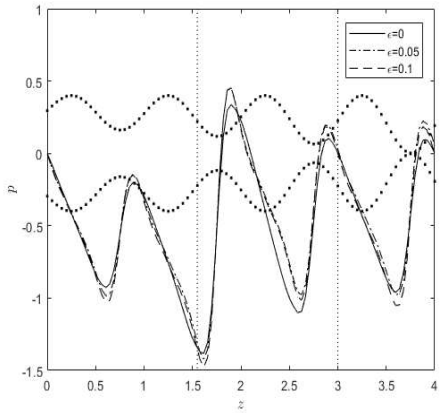

(d)

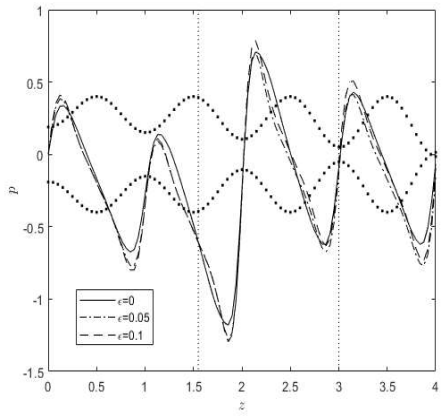

(e)

Figure 6.2: The diagram display the distribution of pressure p along the axial length z when the oesophageal tube is under balloon dilation catheter. The two vertical lines signify the placement of a balloon catheter. The parameters are set as follows: $j_1 = 0.0-0.1$, $\phi = 0.49$, $\alpha = 0.1$, $\mu = 0.2$, $k = 0.01$, $j_1 = 0.1$, $\gamma = 2$, $\gamma_1 = 0.2$, (a) $t = 0$, (b) $t = 0.25$, (c) $t = 0.5$, (d) $t = 0.75$, (e) $t = 1$.

In Figures 6.3(a-e), we observed the effect of the dilating amplitude on pressure distribution in the presence of a balloon catheter. Anatomical measurements of Xia et al. (2009) endorse that a sudden spike in pressure takes place at the lower oesophageal sphincter to grab the bolus wholly into the stomach. It was mathematically modeled by Pandey et al. (2017) in terms of dilating wave amplitude. We have considered this idea in this chapter and observed that its effect is normal near the proximal end of the deflated balloon catheter. In contrast, the change is reflected later in pressure at the balloon-inflated region. We observe higher pressure on increasing its value in the range $k = 0.0 - 0.02$. In the balloon catheter's inflation region, the pressure is much higher than it was earlier. The cycles of the trend of higher pressure distribution continue with time. In comparison to the earlier study of Pandey and co-authors (Pandey et al. (2017), Pandey and Singh (2019), Pandey and Chandra (2022), Pandey and Pandey (2024d), Pandey and Pandey (2024b)), we see a significant change in the impact of dilating amplitude parameter in this study of the balloon catheter. It is concluded that the dilating amplitude parameter plays a crucial role in diagnosing achalasia patients. The reason is that it helps increase

the pressure, so the flow will occur at the inflation point of the balloon catheter. This relieves the patient from pain due to malignant stricture in the oesophagus.

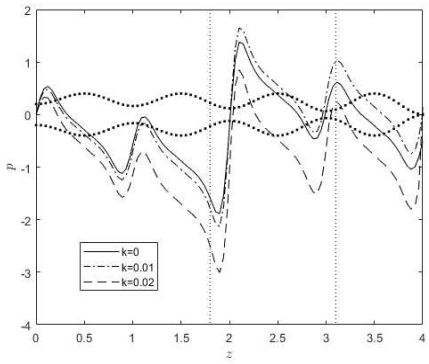

(a)

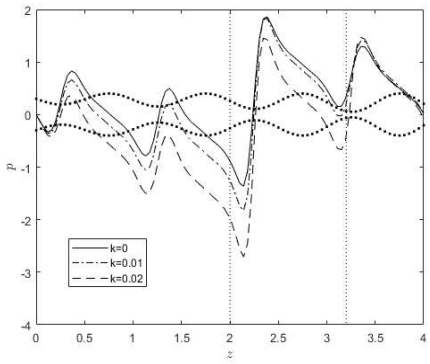

(b)

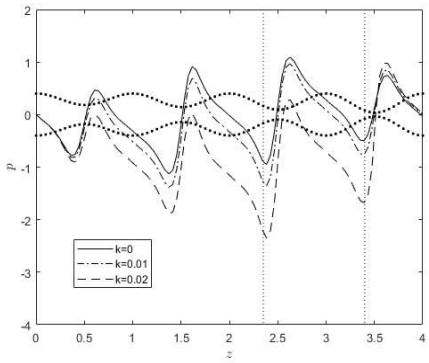

(c)

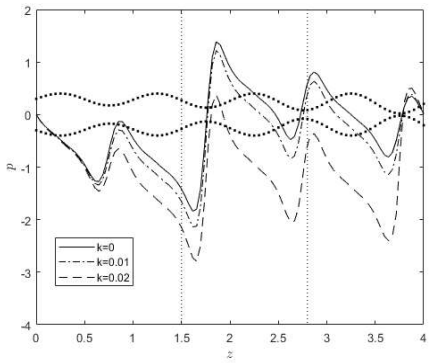

(d)

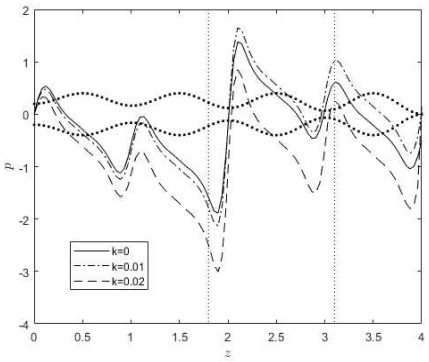

(e)

Figure 6.3: The diagram displays the distribution of pressure p along the axial length z. The affected area in the oesophagus where the pressure spikes due to the dilating amplitude have been shown between the two vertical lines. The parameters are set as follows: $k = 0.0 - 0.02$, $\phi = 0.49$, $\alpha = 0.1$, $\mu = 0.2$, $j_1 = 0.1$, $\gamma = 2$, $\gamma_1 = 0.2$ (a) $t = 0$, (b) $t = 0.25$, (c) $t = 0.5$, (d) $t = 0.75$, (e) $t = 1$.

In Figures 6.4(a-d), we observed the pressure difference with the time-averaged volume flow rate for the parameters such as peripheral layer thickness (α), viscosity (μ), balloon catheter (ϵ), and dilating amplitude parameter (k). We use the equation (6.30) to look into the graphs for the mentioned parameters. Using the equation (6.30), we get the maximum pressure and the maximum time-averaged flow rate by substituting $\bar{Q} = 0$ in equation (6.30). On replacing the Δp by zero in the equation (6.30), we get the maximum time-averaged flow rate. The two are given respectively by equations (6.31) and (6.33). The relation is linear, as shown in (Fig. 6.4a) to (Fig. 6.4d), similar to what Brasseur et al. (1987) obtained for flows without the catheter. This is also validated by the study from Pandey and Pandey (2024d) and Pandey and Pandey (2024b), who investigated the pressure difference with the catheter. Either due to an increase in pressure or the presence of a balloon catheter or both in the oesophagus in the oesophagus, the peripheral layer thickens, which helps to reduce the pressure felt by a patient. Moreover, the impact of the peripheral layer thickness was tested by varying its thickness in the range of 0.5-1.5. It was observed that the flow rate increases if the peripheral layer thickness α is decreased (Fig. 6.4a). Further, we examine the flow rate for different viscosity values, i.e., $\mu = 0.5, 1.0, 1.5$, and find that the flow rate increases with μ (Fig. 6.4b). It is found

that the flow rate is immensely affected and increases with the dilation parameter (Fig. 6.4c). The flow rate increases for the inflated balloon catheter, which is also a sign of relief from the symptoms of dysphagia. The physical interpretation is that the flow rate increases if the peripheral layer is thinner and more viscous. Higher Wave amplitude and larger amplitude dilation increase it further.

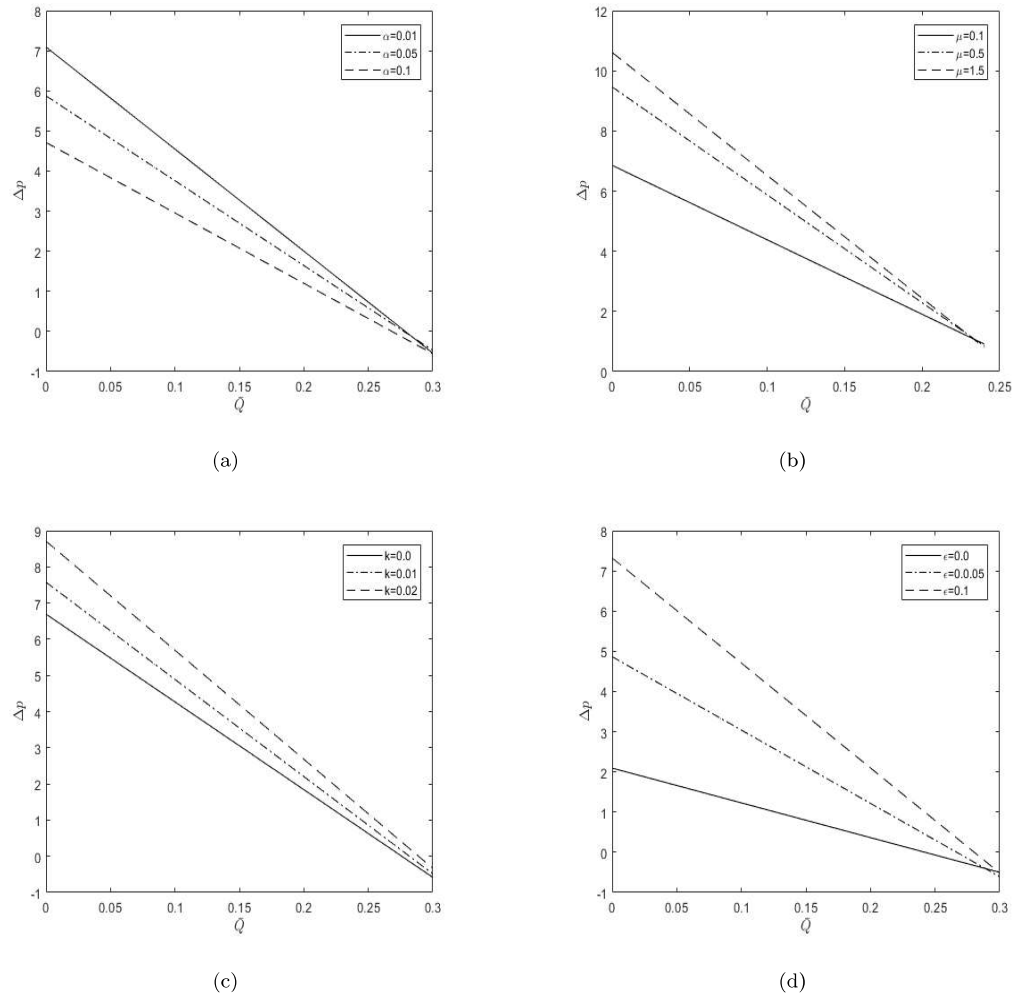

Figure 6.4: The diagram displays the relation between the pressure difference (Δp) with the averaged volume flow rate ($\bar{Q}$). The parameters are set as follows: $\epsilon = 0.1$, $\phi = 0.49$, $\alpha = 0.1$, $\mu = 0.2$, $k = 0.01$, $j_1 = 0.1$, $\gamma = 2$, $\gamma_1 = 0.2$.

Figures 6.5(a-e) are plotted graphs for the axial velocity profile of the peripheral layer through the oesophagus. We observed that due to the higher magnitude of

pressure at the operated region in the oesophagus (Fig. 6.2(a-e)), the velocity of the peripheral layer gets spiked at the same junction. This spiked pressure decreases gradually with time. On broadening the size of the catheter by inflating the balloon in the affected region of the oesophagus, an increase in the velocity is observed. The velocity of the bolus begins at zero and increases at the crest. As the bolus progresses when a patient is fed, it decreases at the trough. The sudden spikes in the graph show that the bolus gets passed quickly as the stricture opens with the help of balloon dilation. We note that the dilating amplitude parameter also affects the velocity profile. The meaning is that the axial velocity increases as the dilating parameter increases, and this helps swallow fluids more easily for Newtonian fluids.

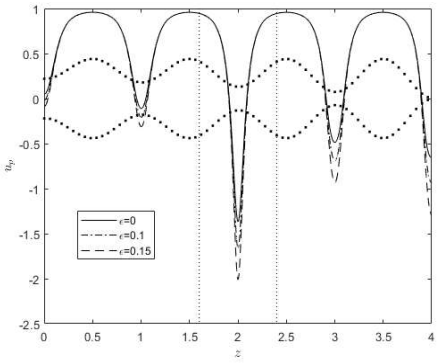

(a)

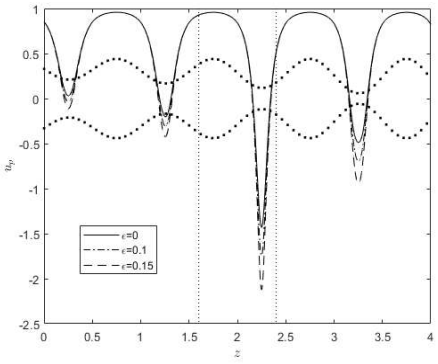

(b)

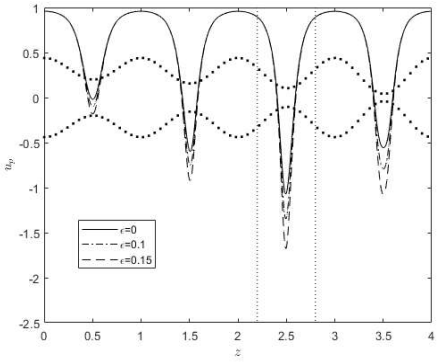

(c)

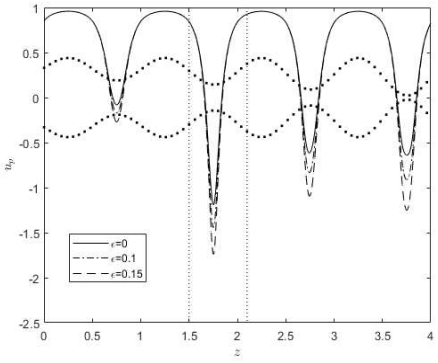

(d)

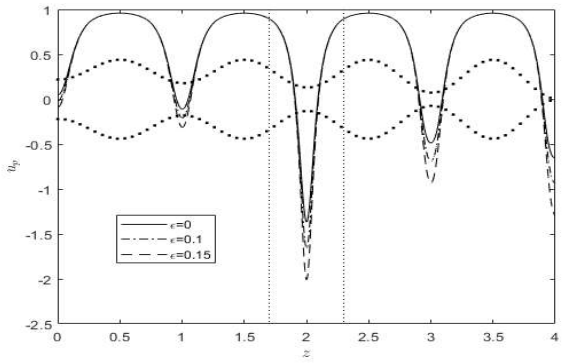

(e)

Figure 6.5: The diagram displays the distribution of peripheral layer velocity u_p along the axial length z. The affected area in the oesophagus where the spikes in the magnitude of velocity due to the inserted balloon catheter have been shown between the two vertical lines. The parameters are set as follows: $\epsilon = 0.0 - 0.02$, $\phi = 0.49$, $\alpha = 0.1$, $\mu = 0.2$, $k = 0.01$, $j_1 = 0.1$, $\gamma = 2$, $\gamma_1 = 0.2$ (a) $t = 0$, (b) $t = 0.25$, (c) $t = 0.5$, (d) $t = 0.75$, (e) $t = 1$.

6.5 Conclusions

The work in this paper is analytical, which provides a mathematical way of pre-diagnosis of swallowing disorders. Results of the constructed model demonstrate that pressure distribution in the human oesophagus with a balloon catheter may be a primary tool for curing Achalasia, including other malignancies. In this analysis, we take the balloon surrounded by a flexible catheter. Moreover, balloon inflation can be caused by water or air. We observed the effects of various parameters on the inflation of a balloon by means of the catheter.

The balloon catheter in the oesophagus can be placed anywhere from the proximal to the distal end. Initially, introducing the catheter to broaden the stricture creates higher pressure. As it progresses towards the stricture site, pressure decreases and rises to push the bolus forward. The pressure increases sharply as the balloon is fully inflated, leading to decreased pressure in the oesophagus and flow start.

It is observed that broadening the balloon catheter's size and increasing the dilating amplitude parameter thickens the peripheral layer. Thickening of the peripheral layer helps increase pressure and is attributed to flow passing through the stricture. Moreover, when increasing the dilating amplitude parameter, the balloon catheter insertion also helps increase the axial velocity in the oesophagus, which shows that the bolus passes quickly as the stricture opens with the inflated balloon.

It is observed that a catheter enclosed within a balloon leads to a higher axial pressure than when it is without a balloon. This is due to the inflation of the balloon catheter at the distal end of the oesophagus. The most vital significance of inserting a novel balloon catheter is that it induces sensitivity and swallowing reflex, which is absent due to Achalasia in the oesophagus, and improves swallowing.